Pharmaceutical Research, Vol. 22, No. 11, November 2005 (© 2005)
DOI: 10.1007/s11095-005-7148-5

Research Paper

Solid Lipid Nanoparticles (SLN) and Oil-Loaded SLN Studied by Spectrofluorometry and Raman Spectroscopy

Katja Jores,[1,2] Annekathrin Haberland,[3] Siegfried Wartewig,[4] Karsten Mäder,[2,5] and Wolfgang Mehnert[1]

Received May 14, 2005; accepted June 28, 2005

Purpose. Recently, colloidal dispersions made of mixtures from solid and liquid lipids have been described to overcome the poor drug loading capacity of solid lipid nanoparticles (SLN). It has been proposed that these nanostructured lipid carriers (NLC) are composed of oily droplets, which are embedded in a solid lipid matrix. High loading capacities and controlled release characteristics have been claimed. It is the objective of the present paper to investigate these new NLC particles in more detail to obtain insights into their structure.

Methods. Colloidal lipid dispersions were produced by high-pressure homogenization. Particle sizes were estimated by laser diffraction and photon correlation spectroscopy. The hydrophobic fluorescent marker nile red (NR) was used as model drug, and by fluorometric spectroscopy, the molecular environment (polarity) was elucidated because of solvatochromism of NR. The packaging of the lipid nanoparticles was investigated by Raman spectroscopy and by densimetry. The light propagation in lipid nanodispersions was examined by refractometry to obtain further insights into the nanostructural compositions of the carriers.

Results. Fluorometric spectroscopy clearly demonstrates that NLC nanoparticles offer two nanocompartments of different polarity to accommodate NR. Nevertheless, in both compartments, NR experiences less protection from the outer water phase than in a nanoemulsion. In conventional SLN, lipid crystallization leads to the expulsion of the lipophilic NR from the solid lipid. Measurements performed by densimetry and Raman spectroscopy confirm the idea of intact glyceryl behenate lattices in spite of oil loading. The lipid crystals are not disturbed in their structure as it could be suggested in case of oil incorporation. Refractometric data reveal the idea of light protection because of incorporation of sensitive drug molecules in NLC.

Conclusion. Neither SLN nor NLC lipid nanoparticles did show any advantage with respect to incorporation rate compared to conventional nanoemulsions. The experimental data let us conclude that NLC lipid nanoparticles are not spherical solid lipid particles with embedded liquid droplets, but they are rather solid platelets with oil present between the solid platelet and the surfactant layer.

KEY WORDS: colloidal carrier; densimetry; fluorometry; nanoemulsion; NLC; Raman spectroscopy; refractometry; SLN; solid lipid nanoparticles.

INTRODUCTION

Colloidal drug carriers offer a number of potential advantages as delivery systems, such as better bioavailability for poorly water-soluble drugs. Beside nanoemulsions, nanosuspensions, mixed micelles, and liposomes, melt-emulsified nanoparticles based on room temperature solid lipids have been developed (1). Advantages of solid lipid nanoparticles (SLN) are the use of physiological lipids, the avoidance of organic solvents, a potential wide application spectrum (dermal, per os, intravenous), and the high-pressure homogenization as an established production method, which allows large-scale production. Additionally, improved bioavailability, protection of sensitive drug molecules from the outer environment (water, light) (2), and even controlled release characteristics were claimed by incorporation of poorly water-soluble drugs in the solid lipid matrix (3,4).

Common disadvantages of SLN are their particle growing, their unpredictable gelation tendency, their unexpected dynamics of polymorphic transitions, and their inherent low incorporation rate because of the crystalline structure of the solid lipid (5–7). It has been claimed that this

[1] Department of Pharmaceutical Technology, Institute of Pharmacy, Free University of Berlin, Kelchstr. 31, 12169 Berlin, Germany.
[2] Institute of Pharmaceutical Technology and Biopharmacy, Martin Luther University Halle Wittenberg, Wolfgang Langenbeck Str. 4, 06120 Halle/Saale, Germany.
[3] Department of Pharmacology and Toxicology, Institute of Pharmacy, Free University of Berlin, Königin Luise Str. 2+4, 14195 Berlin, Germany.
[4] Institute of Applied Dermatopharmacy, Wolfgang Langenbeck Str. 4, 06120 Halle/Saale, Germany.
[5] To whom correspondence should be addressed. (e-mail: maeder@pharmazie.uni-halle.de)

last mentioned drawback can be overcome by oil-loaded solid nanolipids (also described as nanostructured lipid carriers or NLC) (8,9). Liquid lipids solubilize the drug to a much higher extent than solid lipids. In a preferred scenario, the liquid lipids form inner droplets in the solid nanoparticles. In this model, the NLC nanoparticles would provide a high incorporation rate (because of the liquid lipid) and a controlled release (because of the outer solid lipid). It has been postulated that medium chain triglyceride (MCT) molecules can replace glyceryl behenate (GB) molecules in the crystal lattice in a random distribution up to a MCT load of 16% (weight % of total lipid) (8,10). Even higher oil loads up to 38% (weight % of total lipid) are described to be incorporated as MCT clusters inside the solid matrix. It was the objective of the present study to obtain experimental evidence of the postulated structures and to investigate the physicochemical characteristics of the NLC in more detail.

We used the hydrophobic fluorescent stain nile red (NR) as a model drug. Nile red is a solvatochromic dye whose absorption bands vary in shape, position, and intensity with the nature of the solvent (11). Hence, the molecular environment (polarity) of this compound was investigated by fluorometric spectroscopy. The fluorescence of NR is quenched in aqueous medium; therefore, a selective staining of lipophilic compartments is possible (12).

Replacing solid lipid molecules by oily ones in case of oil incorporation implies a change in density of the lipid crystal lattice. To verify this, density measurements and Raman spectroscopy were performed in a noninvasive manner on the nanodispersions. Experiments on refractometry elucidated if NLC are capable to protect sensitive drug molecules from light.

The particle size was assessed by laser diffraction (LD) and photon correlation spectroscopy (PCS).

MATERIALS AND METHODS

Materials

Compritol 888 ATO [International Nomenclature of Cosmetic Ingredients (INCI): tribehenin; United States Pharmacopeia (USP): glyceryl behenate, GB] is a mixture of approximately 15% mono-, 50% di-, and 35% triglycerides of behenic acid (C_{22}), and other fatty acids than behenic acid account for less than 20%. The melting point lies between 69 and 74°C. It was a gift of Gattefossé (Weil-am-Rhein, Germany). Witepsol W25 (HF), donated by Condea (Witten, Germany), is a hardfat mixture (65–80% tri-, 10–35% di-, and 1–5% monoglycerides, fatty acid chain lengths 12–18) with a melting interval from 33.5 to 35.5°C. Miglyol 812 [Deutscher Arzneimittel-Codex (German Pharmaceutical Codex) (DAC), oleum neutrale; Cosmetic, Toiletry and Fragrance Association (CTFA), caprylic/capric triglyceride (caprylic acid, C_8; capric acid, C_{10}), medium chain triglyceride (MCT)] was provided by Caelo (Hilden, Germany). Lutrol F 68 (poloxamer 188; a polyoxyethylenpolyoxypropylen polymer) was donated by BASF (Ludwigshafen, Germany). Nile red (nile blue A oxazone; 9-diethylamino-5*H*-benzo[α]phenoxazine-5-one; NR) was obtained from Sigma (St. Louis, MO, USA).

Methods

Preparation of SLN, Oil-Loaded SLN, and Nanoemulsions

To produce solid lipid nanoparticles, GB was melted at 85°C in a water bath (13). Because of its lower melting point, HF was handled at temperature of 65°C. In case of oil loading, various amounts of MCT were added [2, 4, 10, 15, 20, 25, 30, 40, and 50% (w/w) MCT, referred to the total lipid phase]. The total lipid concentration amounts to 10% in the formulations. For fluorometric measurements, 8.75 μg NR per 35-g sample [corresponding to 0.00025% ($w_{\text{nile red}}/w_{\text{lipids}}$)] was added. The hot lipid phase was given to an aqueous surfactant solution of 2.5% poloxamer 188 of the same temperature, and dispersion was formed using an ultra turrax (IKA, Staufen, Germany) for 30 s at 8,000 rpm. The premix was passed through a Lab 40 high-pressure homogenizer (APV Gaulin, Lübeck, Germany). Three cycles at 85°C (65°C for HF SLN) and 500 bar were performed. Controlled annealing of the dispersions happened in a water bath of 22°C in which the filled silanized glass vials were put. Storage of the samples took place at 22°C, protected from light. The nanoemulsions were prepared in exactly the same manner replacing GB by MCT only. Mixed dispersions (MIXes) were produced by mixing of separately produced solid (SLN) and liquid (NEmu-10%) lipid nanodispersions.

An overview of all investigated formulations is given in Table I.

Particle Size Measurements

To estimate the average diameter and the polydispersity index of the anisometric lipid crystals, photon correlation spectroscopy (PCS; Zetasizer 4, Malvern Instruments, Malvern, UK) under an angle of 90° was used. Before measuring, each sample had to be diluted with demineralized particle-free water to an adequate intensity. Additionally, the laser diffraction method (LD) was used (Coulter LS 230, Miami, FL, USA). Using the polarization intensity differential scattering (PIDS) technology, this instrument is capable of measuring particles down to 40 nm. Each data point is expressed as mean of three experiments performed in triplicate.

Fluorescence Spectroscopy

Emission fluorescence spectra were determined with a Perkin Elmer luminescence spectrometer LS 50 equipped with a 50-Hz xenon flash lamp and a concave grating monochromator. The spectra were recorded at room temperature with both slit widths set at 4 nm. The excitation wavelength was fixed at 546 nm, and the emission spectra were recorded from 550 to 700 nm with a scanning speed of 100 nm/min and a wavelength accuracy of ±1 nm. The simulation of the fluorescence spectra was performed by means of the Origin software from OriginLab Corp., Philadelphia, PA, USA.

Raman Spectroscopy

Raman scattering at an angle of 180° relative to the incident beam was recorded by a Fourier transform Raman spectrometer RFS 100/S (Bruker, Karlsruhe, Germany). The

Table I. Sample Compositions

Sample	Percent lipid (w/w)	Percent GB (w/w)	Percent MCT (w/w)	Percent poloxamer (w/w)	Production procedure
SLN	10	10	0	2.5	Homogenization of dispersions composed of mixtures of molten lipids
NLC-0.2	10	9.8	0.2	2.5	
NLC-0.4	10	9.6	0.4	2.5	
NLC-1.0	10	9	1	2.5	
NLC-1.5	10	8.5	1.5	2.5	
NLC-2.0	10	8	2	2.5	
NLC-2.5	10	7.5	2.5	2.5	
NLC-3.0	10	7	3	2.5	
NLC-4.0	10	6	4	2.5	
NLC-5.0	10	5	5	2.5	
NEmu-0.2%	0.2	0	0.2	2.5	
NEmu-0.4%	0.4	0	0.4	2.5	
NEmu-1%	1	0	1	2.5	
NEmu-2.5%	2.5	0	2.5	2.5	
NEmu-5%	5	0	5	2.5	
NEmu-7.5%	7.5	0	7.5	2.5	
NEmu-10%	10	0	10	2.5	
Micro-GB	10	10	0	2.5	
Micro-MCT	10	0	10	2.5	
Mix-0.2	10	9.8	0.2	2.5	Separate production of GB-SLN and MCT nanoemulsion, followed by mixing of both dispersions in desired ratio
Mix-0.4	10	9.6	0.4	2.5	
Mix-1.0	10	9	1	2.5	
Mix-1.5	10	8.5	1.5	2.5	
Mix-2.0	10	8	2	2.5	
Mix-2.5	10	7.5	2.5	2.5	
Mix-3.0	10	7	3	2.5	
Mix-4.0	10	6	4	2.5	
Mix-5.0	10	5	5	2.5	
Mix-7.5	10	7.5	2.5	2.5	

GB = Glyceryl behenate; MCT = medium chain triglyceride; SLN = solid lipid nanoparticles; NLC = nanostructured lipid carriers.

excitation source was a diode-pumped Nd:YAG laser with an operating wavelength of 1,064 nm. Spectra were acquired with 200 scans and a laser power of 350 mW at sample location. The interferograms were apodized with the Blackman–Harris four-term function and Fourier transformed to give spectra with a resolution of 4 cm^{-1}.

The samples were placed in glass tubes (diameter, 5 mm) and noninvasively analyzed at room temperature. Spectra processing was carried out using the Bruker OPUS software. Raman intensities were determined as integrated band intensities.

Density Measurements

Density was analyzed by an Anton Paar DMA 5000 (AU, Graz, Austria), an instrument based on the detection of density-dependent shifts in the resonance frequency of a flexural resonator filled with the undiluted sample liquid. Each formulation was measured three times at 25°C.

Refractometry

Refractive indices were determined with a refractometer of Zeiss (Oberkochen, Germany), which uses an electric light bulb as light source. Other wavelengths than that one of the sodium vapor lamp (589 nm) are filtered. Measurements were performed at 20°C with the original undiluted nanodispersions, and each data point was registered five times.

RESULTS

Particle Size Measurements

The particle sizes obtained by means of static (LD, PIDS included) and dynamic light scattering (PCS) methods are in the nanometric range (Table II). Nearly unaffected of the concentration of MCT (formulations SLN, NLC-0.2 to NLC-5.0, NEmu-10%), nanoparticles of similar size range were obtained through both size-measuring techniques. Slightly larger particles and an increase in the polydispersity index were observed for SLN and NLC with low oil loads. As the viscosity of MCT compared to GB at temperatures above 70°C was not found to differ (14), better homogenization efficiency owing to lower viscosity can be disregarded as reason for these differences. Moreover, nonspherical platelets as SLN are treated mathematically as spheres, which leads to higher SLN particle size estimates (15). Further inaccuracy is given through the used LD equipment. It combines the methods of diffraction and light scattering to one single result that is not recommended by the current regulatory (16). The nanoemulsion has by far the lowest polydispersity index and a slightly smaller particle size com-

Table II. Particle Size Dependence of SLN on Different Oil Loads, Determined by LD and PCS, Expressed as Median x (x_{min}; x_{max})

Formulation	LD: 50% (V) of all particles smaller than (nm)	LD: 99% (V) of all particles smaller than (nm)	PCS: average particle size (nm)	PCS: polydispersity index (PI)
SLN	163 (140; 216)	614 (591; 711)	250 (215; 287)	0.334 (0.290; 0.381)
NLC-0.2	181 (133; 209)	618 (509; 652)	274 (206; 301)	0.332 (0.252; 0.370)
NLC-0.4	162 (114; 185)	575 (528; 607)	271 (218; 305)	0.292 (0.243; 0.331)
NLC-1.0	173 (148; 205)	572 (532; 634)	276 (241; 338)	0.209 (0.180; 0.225)
NLC-1.5	155 (112; 202)	519 (493; 576)	260 (249; 325)	0.177 (0.153; 0.226)
NLC-2.0	142 (121; 149)	538 (482; 568)	266 (238; 310)	0.165 (0.149; 0.181)
NLC-2.5	139 (102; 173)	568 (480; 550)	262 (238; 311)	0.162 (0.126; 0.191)
NLC-3.0	125 (114; 170)	586 (447; 518)	242 (241; 295)	0.159 (0.104; 0.181)
NLC-4.0	166 (133; 190)	550 (489; 575)	216 (210; 281)	0.155 (0.107; 0.181)
NLC-5.0	168 (145; 200)	544 (515; 562)	217 (212; 244)	0.171 (0.128; 0.189)
NLC-7.5	175 (120; 214)	585 (558; 610)	211 (200; 276)	0.184 (0.130; 0.192)
NEmu-10%	139 (128; 144)	571 (508; 593)	178 (170; 185)	0.143 (0.120; 0.150)
Micro-GB	15,830 (12,690; 15,970)	43,310 (41,050; 45,490)	2,404[a] (1,895; 4,700)	1.000[a] (1.000; 1.000)
Micro-MCT	19,320 (16.450; 19.360)	32,390 (29.980; 32.850)	8,177[a] (4,396; 13,887)	0.668[a] (0.579; 0.857)
Mix-0.2	193 (127; 227)	598 (509; 659)	277 (224; 281)	0.362 (0.313; 0.379)
Mix-0.4	176 (137; 215)	595 (511; 647)	266 (222; 270)	0.334 (0.307; 0.370)
Mix-1.0	165 (125; 192)	600 (552; 672)	269 (218; 272)	0.350 (0.299; 0.390)
Mix-1.5	184 (133; 228)	604 (587; 624)	246 (220; 268)	0.337 (0.318; 0.354)
Mix-2.0	162 (144; 187)	596 (560; 607)	235 (216; 288)	0.331 (0.322; 0.345)
Mix-2.5	154 (128; 188)	554 (536; 649)	225 (207; 262)	0.307 (0.257; 0.331)
Mix-3.0	154 (132: 192)	558 (542; 574)	222 (210; 247)	0.275 (0.265; 0.292)
Mix-4.0	159 (135; 202)	579 (550; 601)	235 (199; 269)	0.318 (0.258; 0.325)
Mix-5.0	153 (105; 187)	578 (514; 640)	208 (185; 219)	0.224 (0.200; 0.236)
Mix-7.5	149 (106; 180)	566 (518; 579)	199 (172; 211)	0.209 (0.193; 0.228)
Wi-SLN	112 (102; 117)	332 (294; 377)	181 (174; 186)	0.165 (0.175; 0.186)

[a] PCS is not a suitable method for particles in the micrometer range.
LD = laser diffraction; PCS = photon correlation spectroscopy.

pared to GB-containing dispersions. Increasing MCT loads did slightly decrease the polydispersity index of the NLC particles; the polydispersity index of the MIX samples was independent from the percentage of MCT. The particle sizes of samples made from physical mixtures of nanoemulsion and nanosuspensions are similar to the values of the nanosuspension. A detailed discussion on particle size and shape correlation can be found in the literature (17).

All measurements were performed at room temperature. Colloidal dispersions made from hardfat did not crystallize at room temperature and represent supercooled melts; therefore, the particle sizes for an emulsion are captured.

The incorporation of a dye had no influence on the particle size. Particle sizes remained unchanged during the measurement period of at least 7 days.

Fluorescence Spectroscopy

The lipophilic benzophenoxazone dye NR is known to show strong fluorescence in a wide range of organic solvents. Its partition coefficient is noted at 196 for chloroform/water (4°C) and less than 1 μg NR is soluble in 1 mL of water (12). However, fluorescence is quenched in aqueous medium. Nile red dispersed into a poloxamer solution looses its fluorescence and becomes a clear colorless solution. Therefore, the disappearance of the fluorescence cannot—in contrast to the claims made by other groups (18)—be discussed as an absence of the nile red in the water phase.

The emission spectra of many fluorescent substances are dependent on the physicochemical properties of the solvents. Nile red shows strong solvatochromism (11), and its absorption band varies in spectral position, shape, and intensity with the nature of the solvent. As a rule, in solvatochromism, the spectrum preserves its essential form, merely shifting to longer or shorter wavelengths if the quantitative relation in a solvent mixture is changed (19). Alterations in the spectral curves cannot only be found in organic solvents of different dielectric constants and refractive indices, but also in various structured colloidal lipid preparations like liposomes and microemulsions (12).

The emission spectra of NR shift to shorter wavelengths with decreasing environmental polarity. Moreover, the fluorescence maxima exhibit the blue shift even proportional to the hydrophobicity of the environment. The blue shift, the quenching phenomenon in water, and the preferential solubility of the dye in lipids account for the selective staining of the colloidal lipid phase and enable to determine the chemical environment of the dye in a noninvasive way.

Confirming this notion, NR-doped SLN made from HF were investigated. Because of the low melting point of HF and because of the colloidal size of the carrier (20,21) at room temperature, HF-SLN possesses a liquid lipid matrix (22) that causes the lack of signals from X-ray diffraction (data not shown). Temperatures well below room temperature (8°C) are required to solidify the lipid matrix within hours to days. Lipid crystallization has a strong impact on the fluorescence properties of NR. The emission maximum moves to a longer wavelength (Fig. 1A). Furthermore, a reduction of the fluorescence intensity is observed. Possible causes of the reduced fluorescence intensity are aggregation of the probe and

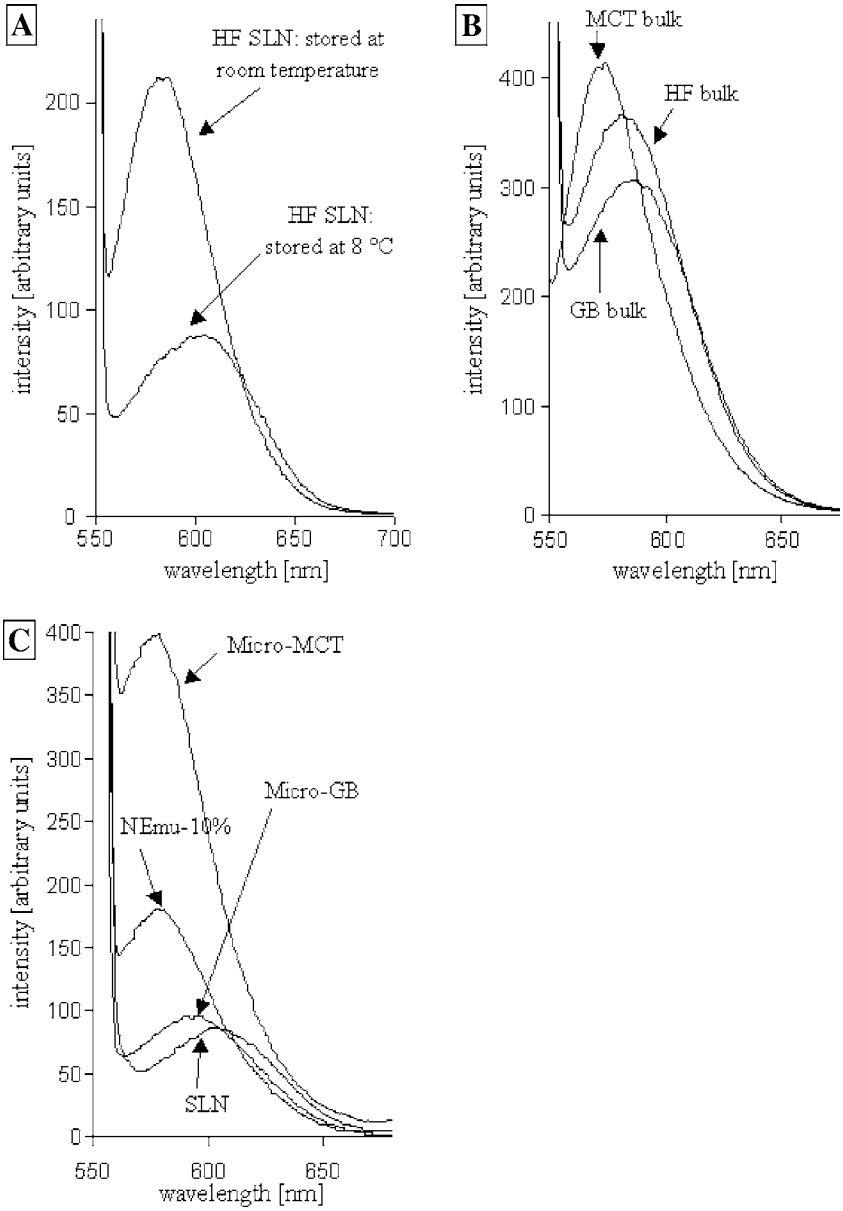

Fig. 1. Fluorescence spectra of nile red (A) in HF solid lipid nanoparticles (SLN) stored at different temperatures, (B) in HF bulk ware, and (C) in aqueous dispersions containing particles of different sizes.

relocation into a more polar environment. Both aggregation and relocation indicate that the solidification of the lipid matrix leads to the expulsion of NR from the lipid matrix.

For a better understanding, the fluorescence properties of NR in bulk were examined (Fig. 1B). The triglyceride MCT creates a more hydrophobic environment than the partial glycerides contained in HF and GB, above all. Intensities decrease in solid lipids; the higher melting GB bulk pronounces even less solubility for NR than the crystal lattice of HF.

The influence of the particle size on the fluorescence properties was investigated by comparing lipid nanoparticles (GB-SLN) with lipid microparticles (Micro-GB). Micro-GB can accommodate slightly higher numbers of NR molecules in more hydrophobic compartment than the nanoparticles (Fig. 1C). Both the GB microparticles and the GB-SLN provide a crystalline matrix with low incorporation capacity, and therefore, the model drug is exposed to water. This finding is consistent with the fact that GB-SLN crystallizes as very thin platelets with a thickness of very few lipid layers. In contrast, the environment of the dye in both kinds of MCT particles is less changed. Micro-MCT protects more NR molecules against quenching than NEmu-10% with considerable larger size-dependent surface area.

The emission spectra of the nanoparticle formulations with varying oil loads are shown in Fig. 2 (upper graphic). Even small changes in the MCT/GB ratio lead to remarkably different fluorescence spectra. The intense signal at 546 nm arises from the reflection of the entering excitation light on

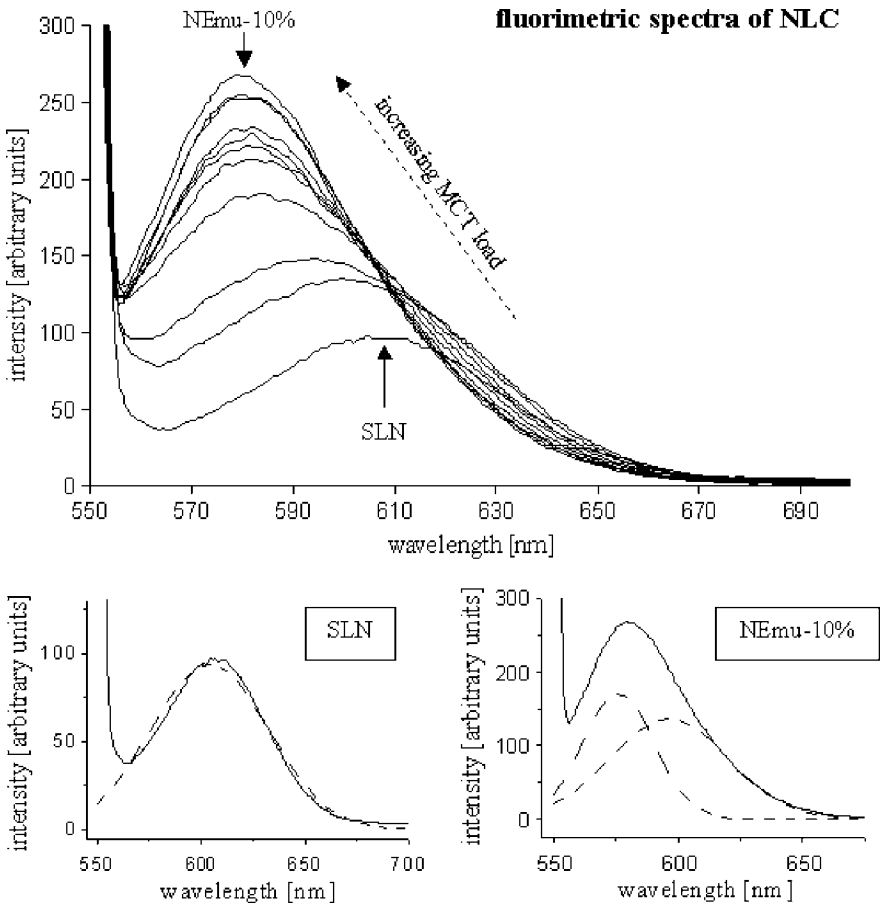

Fig. 2. Fluorimetric spectra of formulations SLN, nanostructured lipid carriers (NLC), NEmu-10% (above), and simulated fits (dashed lines) of the shifted signals of SLN and of NEmu-10% (on the bottom).

the particle surfaces. To obtain exact figures from the shifted peaks, fits are drawn to describe the experimental spectra as good as possible. On closer inspection, two simulated curves are necessary to describe the data exactly in case of NLC samples. The simulation by one (SLN) and two (samples NLC and NEmu-10%) curves, respectively, indicates nanocompartments of different polarity (see Fig. 2, bottom).

The following conclusions can be drawn by a closer look on the peak fits:

1) The fluorescence spectra of pure SLN can be simulated with one fitting curve with a wavelength maximum in a range of 604 nm, which indicates a remarkable polarity [for comparison, NR in acetone yields an emission maximum at 608 nm (12)]. It can be concluded that NR is localized on the particle surface of SLN (probably within the surfactant film on the surface).

2) Oil load creates always an additional second (apolar) compartment at approximately 578 nm for the fluorescent marker [for comparison, NR in chloroform yields an emission maximum at 595 nm and in xylene at 565 nm (12)]. Nile red is either localized on the solid particle surface or accommodated in an oily compartment. The more polar compartment known from SLN disappears suddenly if oil load amounts to more than 20%. Oil load of 20% and more corresponds to an oil concentration enough to host preferentially nearly all marker molecules of the sample. But even in NEmu-10%, a small compartment with medium polarity (at 585 nm) remains where always some NR is localized on the droplet surface, whereas the majority of NR is dissolved in the droplets (578 nm).

3) It can be proven that protecting incorporation characteristics in the solid matrix has failed. The dye aggregates or relocates into a more aqueous environment, leading to quenching of approximately 2/3 of the marker (see loss in intensity in Fig. 3 at SLN in contrast to NEmu-10%, quan-

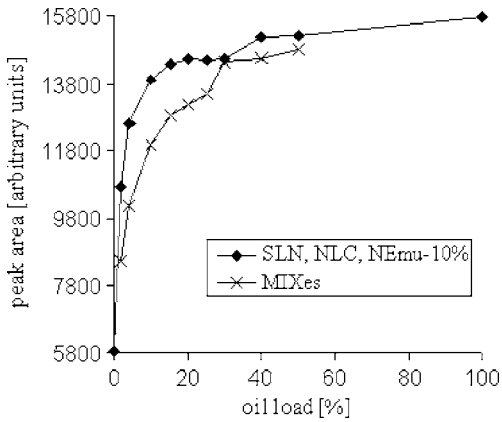

Fig. 3. Dependency of the peak area on the oil content of the samples.

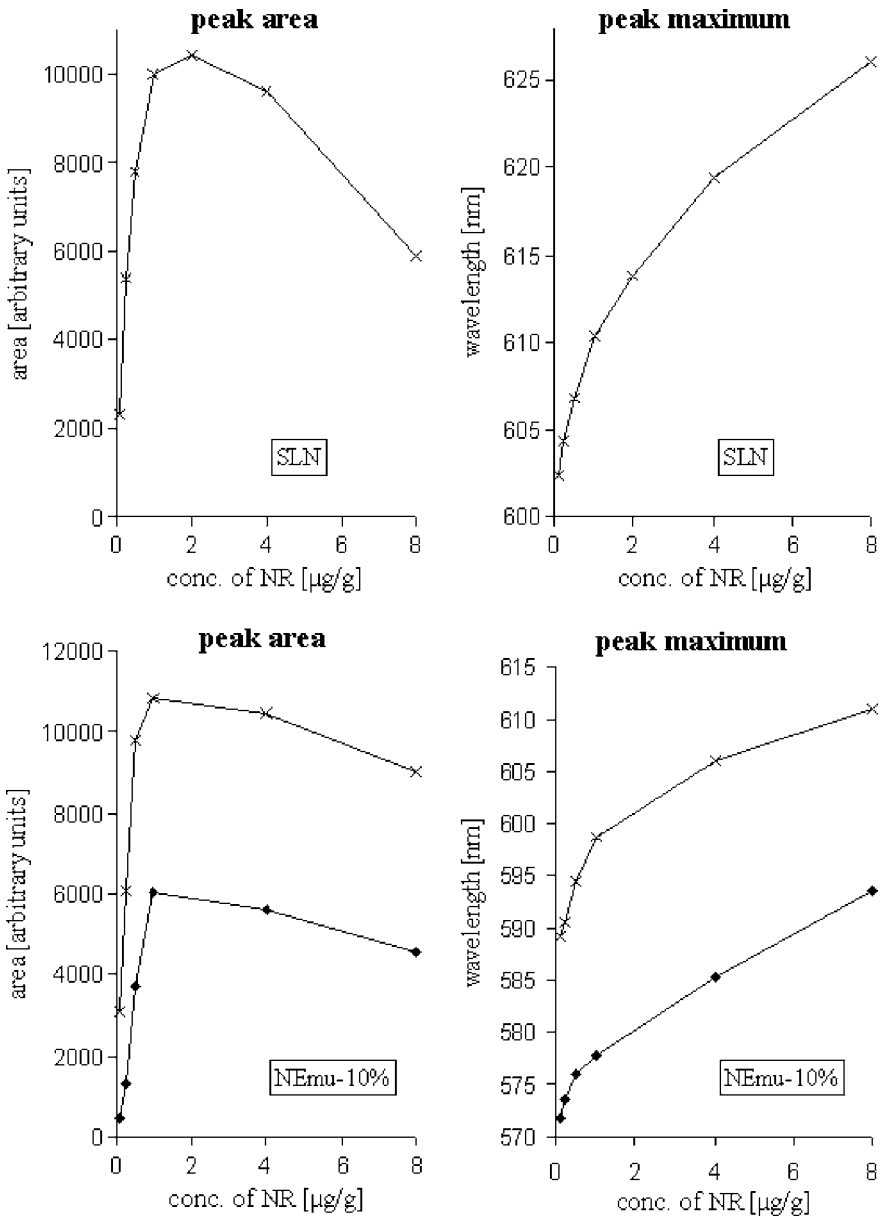

Fig. 4. Influence of nile red concentration on the fluorescence peak area (left side) and peak maxima (right side) for glyceryl behenate–SLN (top row) and medium chain triglyceride (MCT) nanoemulsion (bottom row). As indicated in Fig. 2, the fluorescence signal in MCT is a superposition of two components, and therefore, the concentration dependency for each component is shown.

tified in Fig. 3). Best protection from the outer environment is given in the nanoemulsion.

4) The same quantification of peak areas was performed for MIX samples (Fig. 3). Again, increasing MCT content in the MIX samples increases quenching protection. Above all, regarding samples with low oil content, peak areas were diminished up to 20%, i.e., up to 20% less protected NR in MIXes were found in comparison with NLC. Decreased NR protection in MIXes confirm the short diffusion pathways and rapid distribution of NR into oily compartments of NLC. In MIXes, diffusion possibility from GB to MCT is failed (because of the presence of the aqueous diffusion barrier between liquid and solid particles and because of the quenching effects in water).

It is very important to mention the relation between fluorescence properties and concentration of NR. In Fig. 4, both the emission maxima and the fluorescence intensities vary with the concentration of NR employed. A general rule is that a linear response will be obtained until the concentration of the fluorescent substance is sufficiently large to absorb significant amounts of the exciting light (23). Nonlinear response would provoke artifacts because peak shifting and quenching phenomena could not be correlated accurately to changed sample composition. The employed concentration of 0.25 µg NR per 1 g formulation combines linearity with sufficient fluorescence intensity, if a molecular dissolution of the probe in the lipid is assumed. Crystallization of the lipid will reduce the accommodation capacity for foreign

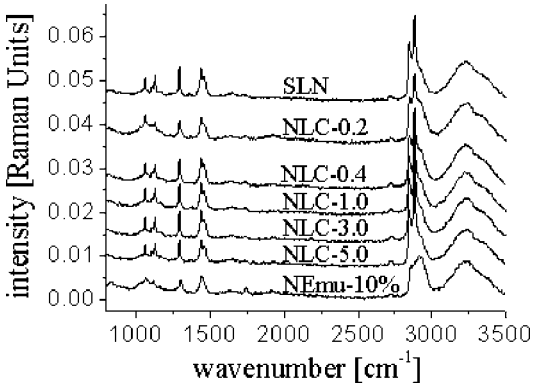

Fig. 5. Raman spectra of different lipid nanodispersions.

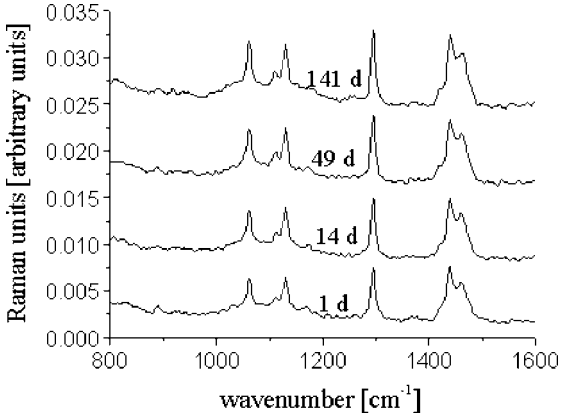

Fig. 6. Raman spectra of the formulation NLC-1.0 during storage process. After 49 days, the sample has already started to build a gel, and after 141 days, it was solid.

molecules and considerably cause expulsion and aggregation of NR.

In summary, the spectrofluorometric studies show a poor incorporation capacity of the marker NR in SLN and NLC. Even the bulk ware of solid lipids cannot accommodate reasonable amounts of the dye. Concerning incorporation capacity and protection from the outer water phase, SLN and NLC are surpassed by a common nanoemulsion. It should be clearly pointed out that the concentration of NR was 0.25 μg/g formulation, so the nanoparticles are only negligibly loaded.

Raman Spectroscopy

Raman spectroscopy detects vibrations of molecules after excitation by an intensive laser beam (24–27).

Figure 5 represents the Raman spectra of SLN, NLC-0.2, NLC-0.4, NLC-1.0, NLC-3.0, NLC-5.0, and NEmu-10%. Solid lipid nanoparticles show a similar pattern as the formulation NLC. In contrast, Raman spectra of the NEmu-10% are clearly different. The Raman band positions observed and their vibrational assignment according to literature data (26,27) are in Table III. Water and poloxamer solutions, respectively, cause only broad peaks at 3,500 cm^{-1} (data not shown), and they are well separated from the lipid signals of interest. Regarding the aspect of oil incorporation in the crystal lattice, bands indicating the order of lipid chains are of high interest. The symmetric stretching modes of the methylene groups at 2,842 cm^{-1} and the sharp band of the asymmetric stretching mode at 2,880 cm^{-1} are indicators for a high degree of conformational order of hydrocarbon chains, and both occur in SLN and in all formulations NLC. In contrast, for the liquid lipid, NEmu-10%, the position of the symmetric CH_2 stretching band is shifted to 2,852 cm^{-1} and the sharp band at 2,880 cm^{-1} disappears, which indicate disordered chains. Additionally, the splitting of the CH_2 scissoring band is less pronounced. Oil loading did not lead to change in order and packing behavior of the lipid chains. Therefore, oil incorporation could not be confirmed by these data.

No significant differences have been found between the experimental spectra of NLC-0.2 and the superposition of the corresponding NEmu-10% and SLN spectra. The Raman spectrum of NLC-0.2 seems as it would be composed of a

Table III. Observed Raman Bands and Assignments to Molecular Vibrations

Band position (cm^{-1})	Assignment	"Diagnostic value"
between 800 and 900	CH_3 rocking	Sharp band at 890 cm^{-1} indicates chain end *trans–trans*
1060	C–C asymmetric stretching	Sharp band indicates 3
1130	C–C symmetric stretching	Sharp band indicates three or more *trans* bonds in sequence
1295	CH_2 twisting	
1420/1440/1465	CH_2 scissoring	Indicator of packing behavior
2842/2852	CH_2 symmetric stretching	Band positions monitor conformational order
2880	CH_2 asymmetric stretching	Sharp band indicates three or more *trans* bonds in sequence

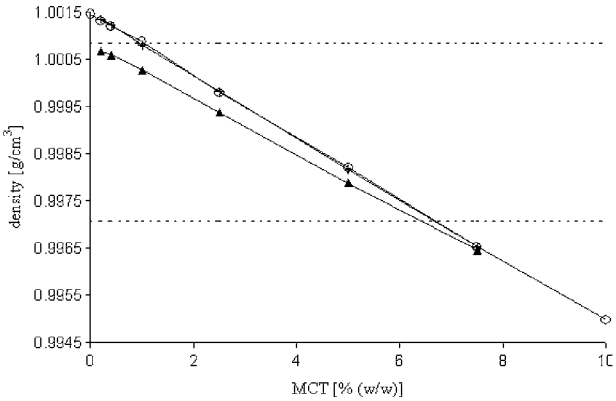

Fig. 7. Dependence of the density on the oil content at 25°C [legend: circle for formulations of different oil loads (SLN, NLC, and NEmu-10%); cross for mixed dispersions (MIXes); triangle for samples NEmu; upper dashed line for a lipid-free poloxamer solution; lower dashed line for water). The density for MCT bulk was determined at 0.941569 g/cm^3. Statistical ranges of each measuring point are too small to be drawn in the figure.

nanoemulsion and of a nanosuspension, without interaction of both lipids.

Despite differential scanning calorimetry, nuclear magnetic resonance, electron spin resonance (ESR), and X-ray measurements, which did not show remarkable changes of the solid lipid dispersions during storage, Raman spectroscopy seems to indicate a further lipid ordering (Fig. 6). The signal at 1,420 cm^{-1} becomes more pronounced, i.e., the packaging behavior is changed. Often, the more pronounced signals are accompanied by gelation of the samples. At the investigated sample on hand (NLC-1.0), gelation has already begun after 49 days, seen by slightly increased viscosity. When stored over nearly 5 months, NLC-1.0 solidifies totally.

Density Measurements

Density is known to vary with the different modifications of a lipid. From earlier examinations (28), we know that oil load does not change the modification of GB.

The density of the samples decreased with increased MCT contents in a strong linear dependency (Fig. 7). Because of the linearity, it can be assumed that the packing density of the GB lattices is not disturbed or changed. Medium chain triglyceride molecules are not incorporated in between the chains of the solid matrix. Moreover, because of the similarity to the densities gained with MIXes, separated nanocompartments consisting of MCT or of GB make more sense. Our results do not support claims of Jenning (29) who proposed a disturbed packaging of the lipids.

Refractometry

Further results on the interaction of the oil with the solid lipid matrix were obtained by refractometry (Fig. 8). Higher MCT contents did lower the refractive indices in a linear dependency. For both samples NLC and MIX, separated nanocompartments (MCT and GB) can be observed. Particles in the given nanometric range interact less pronounced but clearly detectable with light of 589 nm. Advantageous is the bright color of the thin lipid particles for the detection of light refraction.

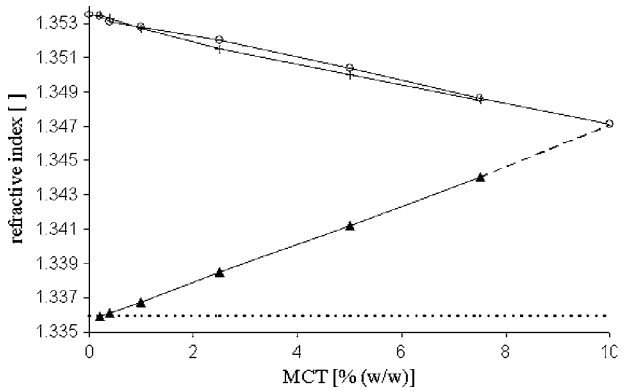

Fig. 8. Dependence of the refractive index on the oil content at 20°C [legend: circle for formulations of different oil loads (SLN, NLC, and NEmu-10%); cross for MIXes; triangle for samples NEmu; horizontal dashed line for a lipid-free poloxamer solution]. The maximal range for median amounts to ±0.0003 that makes possible differences between the two upper curves negligible, but that is too small to be drawn in the graphic.

To proceed on the rough assumption based on the claims in the literature that incorporated oil molecules are covered by the solid lipid matrix and that oil (and sensitive drug molecules inside the oily domains of NLC) are protected from rays of light, oil should not contribute to the refractive index. However, the opposite was found; MCT contributes to the refractive index. Hence, light-sensitive drug molecules are not protected by NLC.

Failing light protection can be stated clearly. Nevertheless, by refractometry, the model of expelled MCT from the solid core cannot be confirmed for certain because little is known on light–particle interaction. Artifacts could be possible because a high penetration depth of light may capture incorporated oil in the solid core itself.

DISCUSSION

Solid lipid nanoparticles are easy to produce at small and large scales. Our investigated samples are stable over a long period of time with respect to particle size, calorimetric behavior, and lipid modification.

The results of our experiments on pure and on oil-loaded GB-SLN are in conflict with the postulated theory of NLC, where drug localization in the solid lipid particle core as well as the incorporation of oily domains of high drug content in the particles has been proposed, but not experimentally proved (9). It should be noted that the measurements were performed with a lipid consisting of glyceride mixtures with a less-ordered matrix in β′-modification. Because of its numerous defects in crystal lattice, GB should facilitate drug incorporation (15,30,31).

The results of the fluorescence experiments show a poor incorporation capacity of the marker NR in SLN and NLC. Even the bulk ware of solid lipids cannot accommodate reasonable amounts of the dye. Concerning incorporation capacity and protection from the outer water phase, SLN and NLC are surpassed by a common nanoemulsion. It should be clearly pointed out that the concentration of NR was 0.25 μg/g formulation; thus, the nanoparticles are only negligibly loaded.

Furthermore, increasing MCT in NLC creates a more hydrophobic compartment for NR, comparable to the oil compartment in MIXes, i.e., a strong indication that MCT molecules in NLC are in close contact to the aqueous phase and not protected in the solid matrix of the particles. However, the results of the fluorimetric measurements permit no final conclusion whether the liquid lipid molecules stay in the inner part of the solid matrix or stick on its outer surface. For further information, Raman spectroscopy and densimetry were carried out.

Measurements performed by densimetry and Raman spectroscopy confirm the idea of intact GB lattices in spite of oil loading. The lipid crystals are not disturbed in their structure as it could be suggested in case of oil incorporation.

By refractometry, the failing light protection for incorporated molecules was elucidated because oil molecules as preferred compartment for lipophilic drug molecules are easily reachable for light quants. Probably, this finding

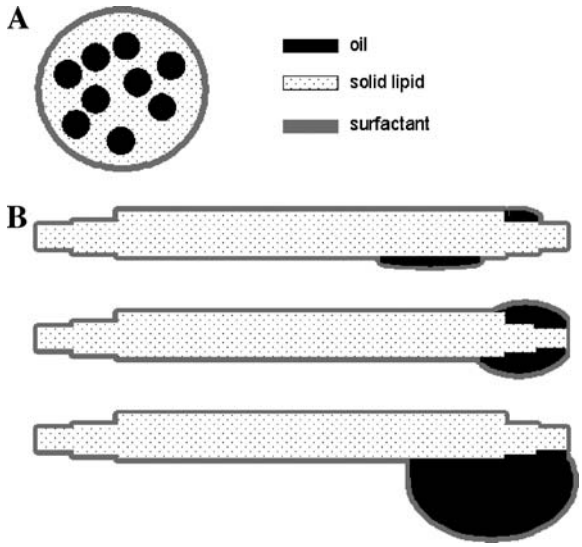

Fig. 9. Schematic structures of NLC; (A) model proposed in the literature, (B) models developed due to current experiments, varying with increasing amount of oil loading.

supports the idea of MCT molecules sticking on the surface of the solid platelets.

CONCLUSION

The results indicate that NLC and SLN show neither a protection from aqueous environment (that could be expected because of the solid matrix) nor a sufficient incorporation rate. Instead of the postulated inner oil droplets (NLC) or incorporated drug molecules (SLN) in the solid matrix, the existence of drug or MCT molecules, respectively, presented on the solid particle surface is more probable in this complex system (Fig. 9). Drug or oil, respectively, are ejected from the molten lipid mix during the lipid crystallization process at the cooling step and aggregate or relocate into a more polar environment. Similar results have been observed by ESR studies. The lipophilic nitroxide Tempolbenzoate did also show aggregation and relocation into a more polar environment due to lipid crystallization in comparable lipid nanodispersions (32,33). The data of the present study are in agreement with results of transmission electron microscopic studies, which show a platelet structure for SLN and a "nanospoon" structure of NLC (17). In NLC, the solid lipid GB crystallizes as very thin platelets and the liquid oil sticks to the solid lipid as a half-drop. The remarkably small thickness of the SLN and NLC particles leads to a very high surface area. Many particles are only 15 nm thin, which translates into only three lipid layers. In other words, for those particles, 2/3 of the solid lipid is localized on the lipid/water interface. The current data indicate that SLN and NLC are not superior to conventional nanoemulsions (17).

ACKNOWLEDGMENT

Katja Jores was supported by Deutsche Forschungsgemeinschaft (DFG).

REFERENCES

1. B. Siekmann and K. Westesen. Submicron-sized parenteral carrier systems based on solid lipids. *Pharm. Pharmacol. Lett.* **1**:123–126 (1992).
2. A. Dingler. Feste Lipid-Nanopartikel als kolloidale Wirkstoffträgersysteme zur dermalen Applikation, PhD Thesis, Berlin, 1998.
3. R. H. Müller, W. Mehnert, J.-S. Lucks, C. Schwarz, A. z. Mühlen, H. Weyhers, C. Freitas, and D. Rühl. Solid lipid nanoparticles (SLN)—An alternative colloidal carrier system for controlled drug delivery. *Eur. J. Biopharm.* **41**:62–69 (1995).
4. R. H. Müller, K. Mäder, and S. Gohla. Solid lipid nanoparticles (SLN) for controlled drug delivery—A review of the state of the art. *Eur. J. Biopharm.* **50**:161–177 (2000).
5. W. Mehnert and K. Mäder. Solid lipid nanoparticles: production, characterization and applications. *Adv. Drug Deliv. Rev.* **47**:165–196 (2001).
6. K. Westesen, H. Bunjes, and M. H. J. Koch. Physicochemical characterization of lipid nanoparticles and evaluation of their drug loading capacity and sustained release potential. *J. Control. Release* **48**:223–236 (1997).
7. K. Westesen and B. Siekmann. Investigation of the gel formation of phospholipid-stabilized solid lipid nanoparticles. *Int. J. Pharm.* **151**:35–45 (1997).
8. V. Jenning, A. F. Thünemann, and S. H. Gohla. Characterisation of a novel solid lipid nanoparticle carrier system based on binary mixtures of liquid and solid lipids. *Int. J. Pharm.* **199**:167–177 (2000).
9. R. H. Müller, M. Radtke, and S. A. Wissing. Nanostructured lipid matrices for improved microencapsulation of drugs. *Int. J. Pharm.* **242**:121–128 (2002).
10. V. Jenning, K. Mäder, and S. H. Gohla. Solid lipid nanoparticles (SLN™) based on binary mixtures of liquid and solid lipids: a ^{1}H-NMR study. *Int. J. Pharm.* **25**:15–21 (2000).
11. A. Hantzsch. Über die Halochromie und "Solvatochromie" des Dibenzalacetons und einfacherer Ketone, sowie ihrer Ketochloride. *Chem. Ber.* **55**:953–979 (1922).
12. P. Greenspan and S. D. Fowler. Spectrofluorometric studies of the lipid probe nile red. *J. Lipid Res.* **26**:781–789 (1985).
13. M. Bockisch. *Nahrungsfette und-öle*, Ulmer, Stuttgart, 1993.
14. A. Fischer-Carius. Untersuchungen an extrudierten und sphäronisierten Matrixpellets mit retardierter Wirkstofffreigabe, PhD Thesis, Berlin, 1998.
15. H. Bunjes, K. Westesen, and M. H. J. Koch. Crystallization tendency and polymorphic transitions in triglyceride nanoparticles. *Int. J. Pharm.* **129**:159–173 (1996).
16. ISO/DIS13320-1. *Korngrößenanalyse—Leitfaden für Laserbeugungsverfahren*, Beuth Verlag, Berlin, Wien and Zürich, 1997.
17. K. Jores, W. Mehnert, M. Drechsler, H. Bunjes, C. Johann, and K. Mäder. Investigations on the structure of solid lipid nanoparticles (SLN) and oil-loaded solid lipid nanoparticles by photon correlation spectroscopy, field-flow fractionation and transmission electron microscopy. *J. Control. Release* **95**:217–227 (2004).
18. C. Olbrich, O. Kayser, A. Lamprecht, C. Kneuer, C. M. Lehr, and R. H. Müller. Interactions of fluorescent solid lipid nanoparticles (SLN) with macrophage-like cells visualized by CLSM. *International Meeting on Pharmaceutics, Biopharmaceutics and Pharmaceutical Technology*, APV/APGI, Berlin, 2000, pp. 331–332.
19. M. M. Davis and H. B. Hetzer. Titrimetric and equilibrium studies using indicators related to nile blue A. *Anal. Chem.* **38**:451–461 (1966).
20. B. Siekmann and K. Westesen. Thermoanalysis of the recrystallization process of melt-homogenized glyceride nanoparticles. *Coll. Surfaces, B* **3**:159–175 (1994).
21. K. Westesen and H. Bunjes. Do nanoparticles prepared from lipids solid at room temperature always possess a solid lipid matrix? *Int. J. Pharm.* **115**:129–131 (1995).
22. S. Liedtke, K. Jores, W. Mehnert, and K. Mäder, Possibilities of non-invasive physicochemical characterisation of colloidal drug carriers, *27th Intern. Symp. Control. Rel. Bioact. Mater.,* Vol. 27, Controlled Release Society, Paris (2000) pp. 1088–1089.

23. S. Udenfriend. *Fluorescence Assay in Biology and Medicine*, Academic Press, New York, San, Francisco, London, 1962.
24. S. Wartewig and R. Neubert. Nicht-invasive Analysenmethoden der Schwingungsspektroskopie in der pharmazeutischen Forschung. *Pharm. Ind.* **64**:863–869 (2002).
25. B. Schrader (ed.), *Infrared and Raman Spectroscopy, Methods and Applications*, VCH, Weinheim, 1995.
26. P. Tandon, G. Förster, R. Neubert, and S. Wartewig. Phase transition in oleic acid as studied by X-ray diffraction and FT-Raman spectroscopy. *J. Mol. Struct.* **524**(27):201–215 (2000).
27. R. Mendelsohn and D. J. Moore. Vibrational spectroscopic studies of lipid domains in biomembranes and model systems. *Chem. Phys. Lipids* **96**:141–157 (1998).
28. K. Jores, W. Mehnert, and K. Mäder. Physicochemical investigations on solid lipid nanoparticles (SLN) and on oil-loaded solid lipid nanoparticles: A NMR- and ESR-study. *Pharm. Res.* **20**:1274–1283 (2003).
29. V. Jenning. Feste Lipid-Nanopartikel (SLN™) als Trägersystem für die dermale Applikation von Retinol: Wirkstoffinkorporation, -freisetzung und Struktur, PhD Thesis, Berlin, 1999.
30. D. Precht. Fat crystal structure in cream and butter. In N. Garti, and K. Sato (eds.), *Crystallization and Polymorphisms of Fats and Fatty Acids*, Marcel Dekker Inc., New York and Basel, 1988, pp. 305–361.
31. V. Jenning and S. Gohla. Comparison of wax and glyceride solid lipid nanoparticles (SLN™). *Int. J. Pharm.* **196**:219–222 (2000).
32. K. Jores, W. Mehnert, and K. Mäder. Physicochemical investigations on solid lipid nanoparticles (SLN) and on oil-loaded solid lipid nanoparticles: a nuclear magnetic resonance and electron spin resonance study. *Pharm. Res.* **20**:1274–1283 (2003).
33. C. Blümer and K. Mäder. Isostatic Ultra High pressure effects on supercooled melts in colloidal triglyceride dispersions. *Pharm. Res.,* accepted (2005).